Malaysian Journal of Chemistry, 2025, Vol. 27(2), 184-196

Synthesis and Characterization of Non-Mesogenic Amide-Ester Derivatives Containing Different Terminal Alkyl Chains

Safiqa Mohram[1], Zuhair Jamain[1]* and Melati Khairuddean[2]
[1]Organic Synthesis and Advanced Materials (OSAM) Research Group, Faculty of Science and Natural Resources, Universiti Malaysia Sabah (UMS), 88400 Kota Kinabalu, Sabah, Malaysia
[2]School of Chemical Sciences, Universiti Sains Malaysia (USM), 11800 Penang, Malaysia
*Corresponding author (e-mail: zuhairjamain@ums.edu.my)

A series of new hybrid amide-ester derivatives was successfully synthesized and characterized. Compounds **2a** and **2b** were differentiated by different alkyl chains lengths ($C_{13}H_{27}$, $C_{15}H_{31}$). The reaction started with 4-nitrobenzoic acid and thionyl chloride in dichloromethane, which was further reacted with 4-aminophenol in the presence of triethylamine to produce intermediate **1**. Next, intermediate **1** underwent an esterification reaction with myristic acid and palmitic acid in the presence of dicyclohexylcarbodiimide (DCC), dimethylaminopyridine (DMAP) and dimethylformamide (DMF) to produce compounds **2a** and **2b**. These compounds were characterized using Fourier transform infrared spectroscopy (FTIR), nuclear magnetic resonance spectroscopy (NMR), and carbon, hydrogen and nitrogen (CHN) elemental analysis. The transition mesophases of these derivatives were determined using a polarized optical microscope (POM). All the compounds produced were non-mesogenic and did not have any liquid crystal properties due to the nonlinearity of their structures.

Keywords: Amide; ester; non-mesogenic; liquid crystal; alkyl chains

Received: December 2024; Accepted: March 2025

The development of a variety of gadgets with unique characteristics and specific functions is a result of the advancement of materials science. Liquid crystalline compounds are one such class of materials that has sparked a great deal of study over the past few decades and resulted in the commercialization of a wide range of materials with exciting uses [1]. The unusual form of matter known as liquid crystals (LCs) combines the characteristics of liquids and crystals. They are substances that have a liquid-like flow but also exhibit molecular order and alignment, much like crystalline solids [2]. LCs are incredibly valuable in many technological applications, particularly in display technology [3-5].

Linking units play a crucial role in liquid crystals by preserving the linear nature of the core and ensuring compatibility with the overall structure. Additionally, the linking unit situated between ring systems helps extend the length of the molecules [6]. Interestingly, these linking units also affect the polarizability and flexibility of the molecules [7]. Depending on their properties, linking units can either add polarity or serve as non-polar groups [8]. The presence of linking units is believed to either enhance or reduce the polarizability of molecular compounds that exhibit LC behaviour [9].

Amide compounds are not very common in low-molecular-weight LCs. Amides can be classified as primary, secondary, or tertiary, depending on the nature of the N-substituents. Secondary amides can display LC phases, but they often come with high melting points. This is due to the strong hydrogen bonding found in these compounds [10]. Amide groups are utilized in LC phases to stabilize the arrangement of columns. The ester linking unit is frequently used in calamitic LCs because it is stable and simple to make. Additionally, the carbonyl group's polarizability aids in the formation of smectic phases and a lamellar order [11]. However, the direction of the polar ester linking group that connects the aromatic rings can be reversed, which has an essential effect on the mesomorphic behaviour of molecules [12].

The relationship between the molecular structure, which encompasses the core system, linking units, and terminal groups, plays a vital role in the study of LCs. The behaviour of ester or amide units is affected by LCs. Liquid crystalline properties are determined by the presence of a central connection and end groups. Aromatic nuclei are commonly found in compounds with short central linkages, such as amides and esters [13]. Mesogens that consist of both carbocyclic and heterocyclic aromatic residues can be found in longer molecules. The mesophase type is determined by the terminal group. The molecular shape and length of the terminal chain are the main factors in developing new LC compounds with specific types of molecular organization within a particular temperature range [14,15]. Higher temperatures can lead to the breakage of labile bonds, disintegration, decomposition, and loss of LC properties [16]. The melting point is generally dependent on the molecular structure because attractive forces within the crystal lattice are influenced by the thermal stability of the solid state. In the mesophase, molecules exhibit easy rotation, resulting in dipole-dipole moments and dispersion forces [17,18].

Even though extensive research has been performed on liquid crystal compounds over the years, the phase properties of amide and ester compounds with unique properties attached to different terminal alkyl chains have still not been fully explored. The examination of the correlation between the core system, connecting unit, and terminal group as the primary factors influencing mesophase transition in compounds is inadequate and lacks sufficient documentation. Hence, this research focused on preparing and determining the LC properties of new amide and ester linking unit derivatives for the LC database.

EXPERIMENTAL

Chemicals and Materials

The chemicals and solvents used in this study were 4-nitrobenzoic acid, 4-aminophenol, palmitic acid, myristic acid, thionyl chloride, dicyclohexylcarbodiimide, dimethylaminopyridine, dimethylformamide, dichloromethane, triethylamine, tetrahydrofuran, and n-hexane. All the chemicals were purchased from Acros Organics (Geel, Belgium), BDH laboratory (British Drug Houses) (Nichiryo, Japan), QREC (Asia) (Selangor, Malaysia), Merck (Darmstadt, Germany) and Sigma-Aldrich (Steinheim, Germany), and used without purification.

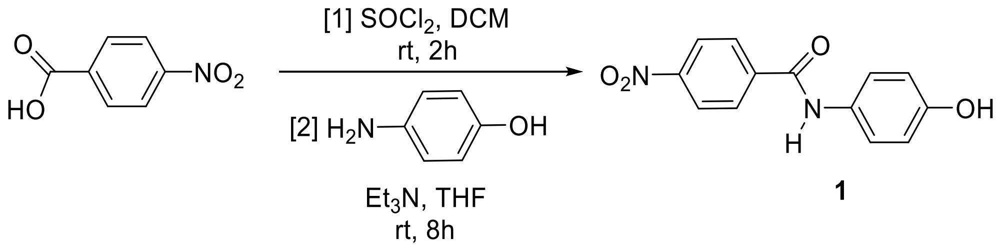

Scheme 1. Formation of intermediate **1**.

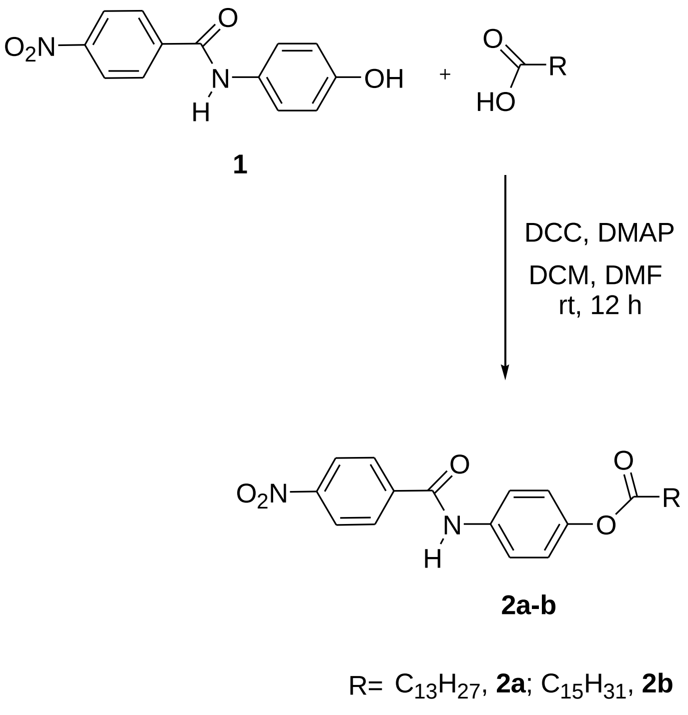

Scheme 2. Esterification of compounds **2a-b**.

Characterization Methods

In this study, thin layer chromatography (TLC) was employed to monitor the reaction progress and assess the purity of the products. The eluent used was a 10:90 ratio of ethyl acetate to hexane. FTIR spectroscopy (PerkinElmer, Waltham, MA, USA) was used to determine the functional groups present in the samples, with scans performed within the range of 400 to 4000 cm^{-1}. The structures of all synthesized compounds were elucidated using NMR spectroscopy (Bruker, Coventry, UK), while the purity of the compounds was verified with a CHN elemental analyzer (Perkin Elmer, Waltham, MA, USA). The liquid crystalline behaviour of the compounds was examined by polarized optical microscopy (POM) (Linkam, London, UK) using an Olympus BX53 system with a scan rate of 10 °C.

Synthesis Summary

In this study, two schemes were involved: the formation of intermediate **1**, and the esterification reaction producing **2a-b**. The experiment began with 4-nitrobenzoic acid undergoing a two-step process. The first step used thionyl chloride with dichloromethane. This was followed by the second step with 4-aminophenol in the presence of triethylamine to produce intermediate **1** as shown in Scheme 1 [19,20]. Next, intermediate **1** underwent an esterification reaction, by reacting with myristic acid (palmitic acid?) in the presence of dicyclohexylcarbodiimide, DCC, dimethylaminopyridine, DMAP, and dichloromethane, DMF to produce compounds **2a-b** as illustrated in Scheme 2 [21,22].

Synthesis of 4-(4-hydroxyphenyl)-4-nitrobenzamide, 1

In a 100 mL round bottom flask, 0.03 mol of 4-nitrobenzoic acid and 0.09 mol of thionyl chloride were combined to generate an acid chloride. Achieving a clear solution necessitated stirring the mixture at room temperature for two hours. Addition of the 0.03 mol solution of 4-aminophenol dropwise in 20 mL of THF resulted in a white precipitate. Subsequently, 0.09 mol of triethylamine (Et$_3$N) was introduced, and the mixture was stirred for 8 hours. The progression of all reactions was monitored using TLC. The precipitate was filtered, and the filtrate collected. Following drying, the resulting product was recrystallized from n-hexane.

Yield = 6.11 g (78.98 %), dark black. **FTIR (cm^{-1})**: 3309 (N-H stretching), 3111 (O-H stretching), 1684 (C=O stretching), 1600 (aromatic C=C stretching), 1530 & 1344 (N=O), 1276 (C-N stretching) and 1106 (C-O stretching). **^{1}H NMR (500 MHz, DMSO-d_6)** δ, ppm: 10.06 (s, 1H), 8.29 (d, J=10 Hz, 2H), 8.06 (d, J=10 Hz, 2H), 8.00 (d, J=10 Hz, 2H), 6.84 (d, J=10 Hz, 2H). **^{13}C NMR (125 MHz, DMSO-d_6)** δ, ppm: 166.77, 162.55, 146.89, 143.12, 130.75, 125.80, 124.47, 120.50, 113.96. **CHN elemental analysis**: Calculated for $C_{13}H_{10}N_2O_4$: C: 60.47 %, H: 3.90 %, N: 10.85 %. Found: C: 60.35 %, H: 3.85 %, N: 10.79 %.

Synthesis of Compounds 2a-b

In a 100 mL round bottom flask, 0.006 mol of intermediate **1** in 10 mL DMF was combined with 0.006 mol of myristic acid, 0.006 mol of dicyclohexylcarbodiimide (DCC), 0.006 mol of dimethylaminopyridine (DMAP), and 50 mL of dichloromethane (DCM). The mixture underwent stirring for one hour at 0 °C, followed by an additional 12 hours at room temperature. Throughout the stirring process, a cloudy white solid was observed. The reaction progress was monitored using TLC. Upon completion, the precipitate was filtered, and the filtrate was collected. The filtrate underwent evaporation, resulting in the formation of a precipitate that was subsequently purified via recrystallization, yielding a white powder, **2a**. The same synthetic method was applied to produce compound **2b**.

*4-(4-nitrobenzamido)phenyl tetradecanoate, **2a***

Yield = 2.11 g (74.96 %), white powder. **FTIR (cm^{-1})**: 3319 (N-H stretching), 2923 and 2850 ($Csp^3 - H$ stretching), 1622 (C=O stretching), 1533 (aromatic C=C stretching), 1443 and 1309 (N=O), 1235 (C-N stretching) and 1081 (C-O stretching). **^{1}H NMR (500, DMSO-d_6)**. δ, ppm: 10.25 (s, 1H), 8.16 (d, J=10 Hz, 2H), 7.96 (d, J=10 Hz, 2H), 7.92 (d, J=10 Hz, 2H), 7.00 (d, J=10 Hz, 2H), 1.70-1.74 (m, 2H), 1.37-1.43 (m, 2H), 1.22-1.33 (m, 20H), 0.82 (t, J=5, 3H). **^{13}C NMR (125 MHz, DMSO-d_6)** δ, ppm: 166.31, 162.52, 145.90, 143.32, 137.15, 135.02, 130.24, 124.86, 120.61, 114.97, 31.54, 29.22, 29.21, 29.18, 29.16, 29.15, 28.93, 28.88, 25.74, 22.27, 13.99. **CHN elemental analysis**: Calculated for $C_{27}H_{36}N_2O_5$: C: 69.21 %, H: 7.74 %, N: 5.98 %. Found: C: 69.18 %, H: 7.70 %, N: 5.95 %.

*4-(4-nitrobenzamido)phenyl palmitate, **2b***

Yield = 2.98 g (74.09 %), white powder. **FTIR (cm^{-1})**: 3295 (N-H stretching), 2925 and 2852 ($Csp^3 - H$ stretching), 1644 (C=O stretching), 1530 (aromatic C=C stretching), 1449 and 1338 (N=O), 1236 (C-N stretching) and 1079 (C-O stretching). **^{1}H NMR (500, DMSO-d_6)**. δ, ppm: 10.25 (s, 1H), 8.17 (d, J=10 Hz, 2H), 7.96 (d, J=10 Hz, 2H), 7.92 (d, J=10 Hz, 2H), 7.00 (d, J=10 Hz, 2H), 1.68-1.74 (m, 2H), 1.37-1.43 (m, 2H), 1.23-1.34 (m, 24H), 0.82 (t, J=5 Hz, 3H). **^{13}C NMR (125 MHz, DMSO-d_6)** δ, ppm: 166.31, 162.53, 145.91, 143.33, 138.55, 135.43, 130.25, 124.86, 120.61, 114.98, 31.55, 29.25, 29.23, 29.22, 29.19, 29.18, 29.16, 29.15, 28.94, 28.89, 25.75, 22.28, 14.00. **CHN elemental analysis**: Calculated for $C_{29}H_{40}N_2O_5$: C: 70.13 %, H: 8.12 %, N: 5.64 %. Found: C: 70.08 %, H: 8.11 %, N: 5.60 %.

RESULTS AND DISCUSSION

FTIR Spectra

The FTIR spectrum of compound **2a** showed that it had functional groups that were very similar to compound **2b**. The discussion of functional groups in compounds **2a** and **2b** will focus on the amide group, nitro group, aromatic ring stretching, carbonyl group stretching specifically of the amide group, ester group, and C-H stretching of the *sp3* orbital of the alkane chain.

The final compound differed from intermediate **1** by the inclusion of an ester group and a lengthy alkyl chain. Therefore, effective addition was confirmed by observing the presence of C-O stretching and *sp3* C-H stretching bands in the FTIR spectrum. The presence of absorption bands at 3319 cm^{-1} indicating N-H stretching vibrations showed that compound **2a** had an amide linking unit. N-H amide stretching bands usually appear at around 3300 to 3400 cm^{-1}. The peak at 1235 cm^{-1} in the IR spectrum of the synthesized compound was assigned to the C-N stretching of the amide group.

A strong peak below 3000 cm^{-1} showed the presence of alkane C-H *sp3* stretching. This appeared at a slightly lower frequency due to the symmetrical nature of the compound. The symmetric mode generates a smaller dipole moment and intensity compared to the asymmetric mode [23]. Thus, the alkane C-H stretching vibrations were observed at 2850 and 2923 cm^{-1} in the spectrum. These peaks showed symmetric (sym) and asymmetric (asym) stretching modes for the methylene and methyl groups [24].

Based on its intensity and position, the peak observed at 1622 cm^{-1} was identified as a carbonyl group, namely the C=O stretching vibration. However, the presence of a band within the range of around 1600 to 1750 cm^{-1} confirmed that this band belonged to the amide group [25]. The precise location of the C=O group showed a downshift in frequency due to the conjugation effect, as it was positioned next to an unsaturated benzene ring. Consequently, the π electrons in the C=O and C=C bonds in the aromatic ring became delocalized. The process of conjugation enhanced the single bond character in the C=O and C=C bonds of the resonance hybrid. As a result, the force constant of these bonds decreased, leading to a reduction in the C=O absorption frequency [26].

C=C stretching bands for aromatic rings are frequently found between 1600 to 1450 cm^{-1}. In this case, the peak was at 1533 cm^{-1}, because the compound contained an amide group, which caused the lower absorption frequency. The substitution pattern on the aromatic ring could be determined by observing the peak at 890 cm^{-1} which indicated the out-of-plane and aromatic ring bending mode. The band also indicated that all the final compounds had *para-* disubstituted (1,4-disubstituted) rings in the structure.

The nitro group was indicated by strong peaks in the region of 1350-1550 cm^{-1}. The stretching vibrations of the N=O bonds, both symmetric and asymmetric, are the most noticeable peaks connected to the nitro group (Beal & Brill, 2005). It is common for symmetric stretching to occur between 1340 and 1380 cm^{-1}, and asymmetric stretching to occur between 1520 and 1580 cm^{-1}. Figure 4.2 showed typically well-defined and strong peaks at 1309 and 1443 cm^{-1}.

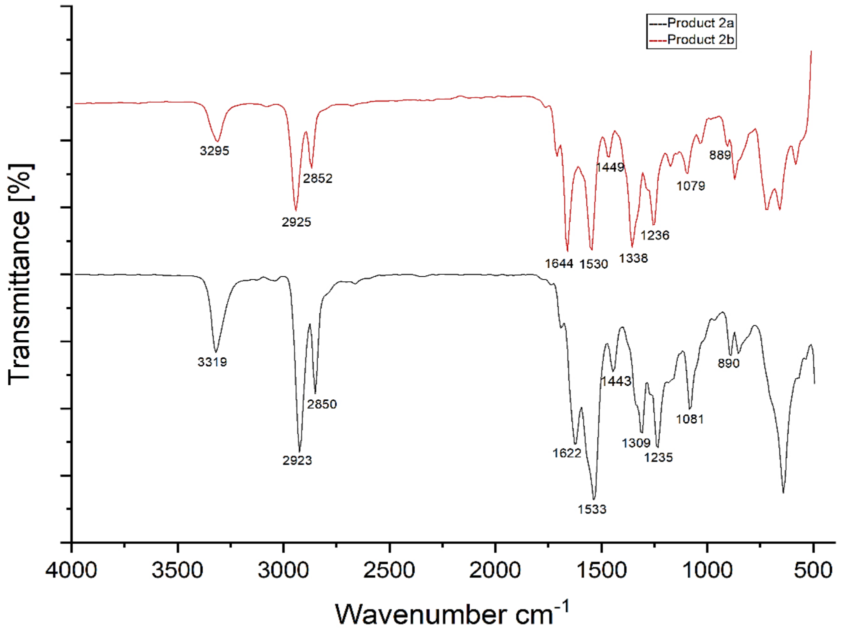

Figure 1. FTIR spectra of compounds **2a-b**.

The intense peaks observed in the spectral region of 1000 to 1300 cm⁻¹ were attributed to the presence of ester functional groups, indicating the occurrence of C-O stretching vibrations. It was also clear that the peak at 1081 cm⁻¹ corresponded to the C-O stretching vibration of the ester group. This indicated the successful formation of an ester compound.

Figure 1 shows the overlaid FT-IR spectra of the final compounds. The summarized FTIR vibrational stretching (cm^{-1}) data of compounds **2a** and **2b** are tabulated in Table 1. It may be concluded that both compounds had almost the same spectral wavenumbers and peak intensities. This was because **2a** and **2b** consisted of the same functional groups attached to alkyl chains of different lengths.

Table 1. The summarized FTIR data for compounds **2a-b**.

Functional Group	**Vibrational Stretching (cm^{-1})**	
	2a	**2b**
N-H stretching	3319	3295
$Csp^3 - H$ stretching	2923 & 2850	2925 & 2852
C=O stretching	1622	1644
Aromatic C=C stretching	1533	1530
N=O	1443 & 1309	1449 & 1338
C-N stretching	1235	1236
C-O stretching	1081	1079

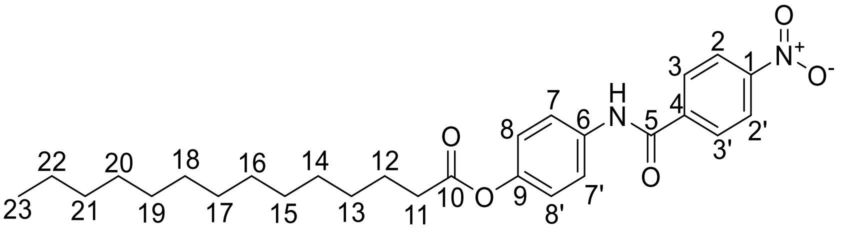

Figure 2. Chemical structure of compound **2a** with complete atomic numbering.

Table 2. Summarized ¹H NMR data for compound **2a**.

Proton(s)	**Number(s) of H**	**Coupling constant, J (Hz)**	**Chemical shift, δ**	**Multiplicity of signal (s)**
NH	1	-	10.25	s
H2/H2’	2	10	8.16	d
H3/H3’	2	10	7.96	d
H7/H7’	2	10	7.92	d
H8/H8’	2	10	7.00	d
H11	2	-	1.70-1.74	m
H12	2	-	1.37-1.43	m
H13-H22	20	-	1.22-1.33	m
H23	3	5	0.82	t

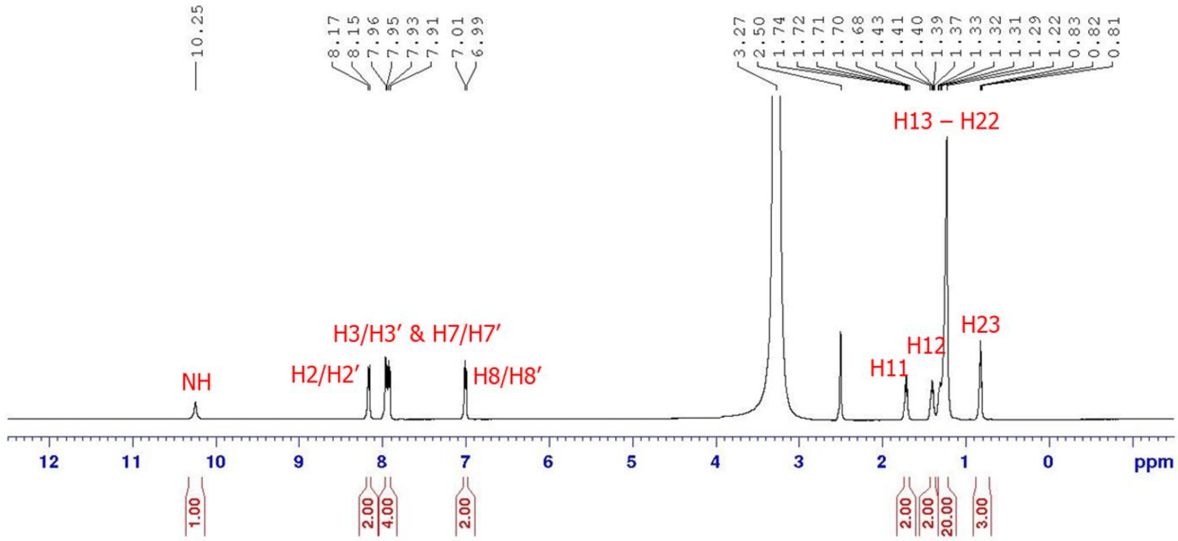

Figure 3. ^{1}H NMR (500 MHz, DMSO-d_6) spectrum of compound **2a**.

NMR Spectra

^{1}H NMR

The structure of compound **2a** is shown in Figure 2, with complete atomic numbering. The chemical shift, δ (ppm) and coupling constant (J) data for compound **2a** are tabulated in Table 2 and its ^{1}H NMR spectrum is illustrated in Figure 3.

When comparing intermediate **1a** with compound **2a**, the only notable difference was the addition of an ester. In the ^{1}H NMR spectrum of compound **2a** (Figure 3), a singlet in the downfield region at δ 10.25 ppm was assigned to the amide group. Four distinguishable doublets within δ 6.99 – 8.17 ppm (H2/H2', H3/H3', H7/H7' and H8/H8') were assigned to the aromatic protons. One of these signals integrated to four protons and appeared as two overlapping doublets (H3/H3' and H7/H7'). The chemical shifts of H2/H2' were higher than those of H3/H3' due to the anisotropic and resonance effects of an electron-withdrawing nitro group attached at the ortho position to H2/H2'. An amide carbonyl has a weaker electron-withdrawing strength through resonance than a nitro group [27,28]. This phenomenon caused the H2/H2' signals to appear at the deshielded region due to lower electron density around these protons.

Similar explanations apply to the deshielding effects observed in H3/H3' and H7/H7'. H3/H3' was slightly more distant from the nitro group, resulting in a lower deshielding effect compared to H2/H2'. For H8/H8', two doublets appeared in a more shielded region than H3/H3', H2/H2', and H7/H7'. This was because these protons were positioned further away from the nitro and carbonyl groups, leading to a weaker inductive effect than the resonance effect [29].

In the upfield region at δ 1.70-1.74 ppm, the presence of the α-position of H11 and the β-position of H12 indicated that the β-carbon and β-hydrogen were more shielded due to lower electron density around the β-carbon, as per the theory. The π-electrons of benzene created an anisotropic field, interacting with the β-hydrogen and causing further deshielding [30]. The subsequent proton in the alkyl chain exhibited a chemical shift at δ 1.37-1.43 ppm as a doublet (H12), while signals in the range of δ 1.22-1.33 ppm were assigned to the remaining protons (H13-H22) in the alkyl chain. Lastly, a triplet upfield at δ 0.82 ppm was assigned to H23.

The NMR spectra of compound **2b (**Figure 4) exhibited a pattern similar to that of compound **2a**, with a slight variation, particularly in the δ 1.23 - 1.34 ppm range. This difference arose from the longer alkyl chain attached to **2b**, leading to a higher number of protons compared to **2a**.

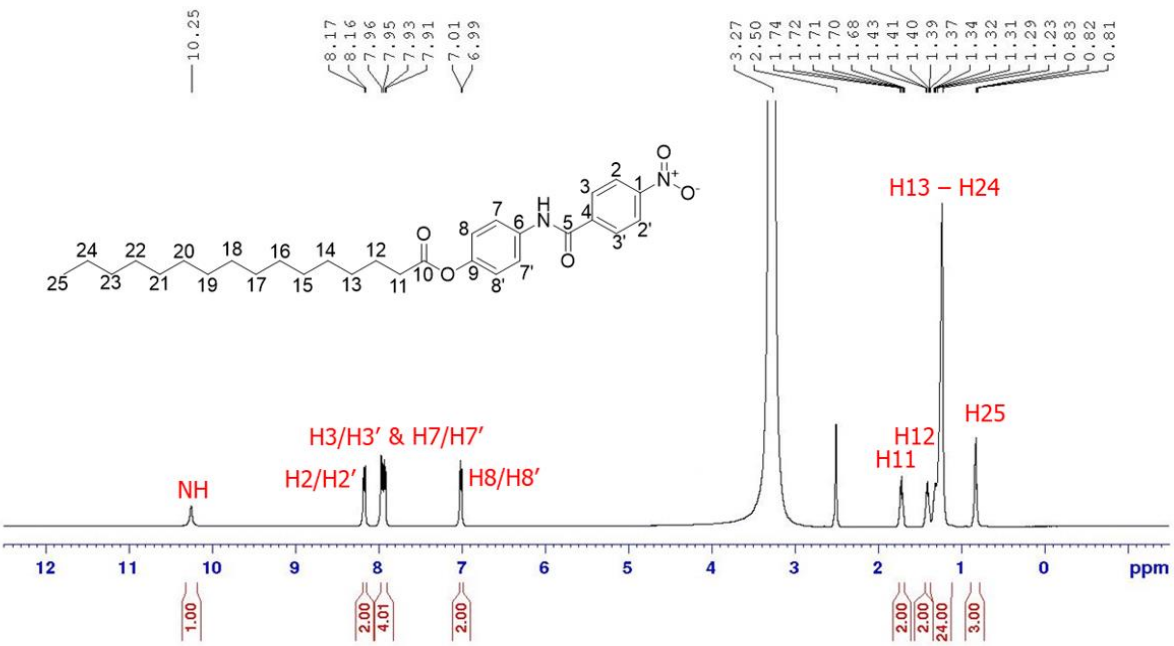

Figure 4. ^{1}H NMR (500 MHz, DMSO-d_6) spectrum of compound **2b**.

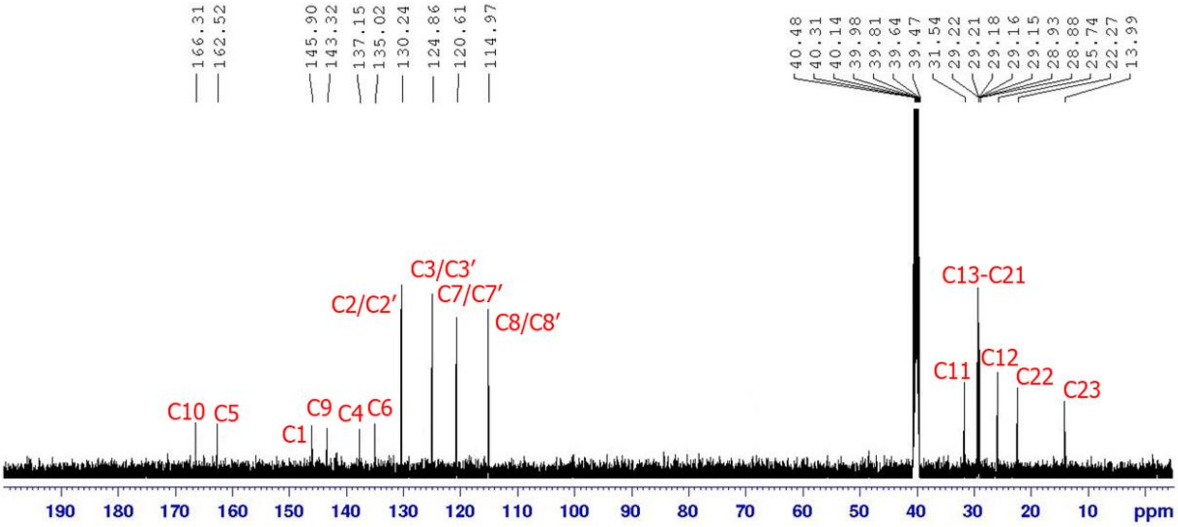

Figure 5. ^{13}C NMR (125 MHz, DMSO-d_6) spectrum of compound **2a**.

^{13}C NMR

The ^{13}C NMR spectrum of compound **2a** (Figure 5) showed carbon signals comprising two carbonyls, four methine, 6 quaternary, 15 methylene, and one methyl carbons. The most downfield peak was assigned to the carbonyl carbon of the ester linkage, which resonated at δ 166.31 ppm (C10), while the carbonyl carbon of the amide group resonated at δ 162.52 ppm (C5). These carbons were most deshielded due to the highly electronegative oxygen atom directly attached to the carbon of the carbonyl group. Oxygen has electron-withdrawing properties thus it pulls electron density away from carbon and toward itself. As electronegative atoms draw electrons towards themselves, they extract electrons from adjacent carbon atoms, leading to the deshielding of those carbons which thus resonate at a lower magnetic field [31].

Other signals at δ 145.90, 143.32, 137.15, and 135.02 ppm were assigned to the quaternary carbons C1, C9, C4, and C6, respectively. The nitro group (-NO_2) contains electronegative oxygen and nitrogen atoms. Both atoms withdraw electron density from the carbon atoms in the aromatic ring. This electron-withdrawing effect resulted in the deshielding of the carbon atoms in the aromatic ring, leading to a higher chemical shift in the classification of Ar-X. The electronegative oxygen atom in aryl ether may deshield the adjacent carbon to some extent, but it might not be as strong as the nitro group [32]. The aryl amine group (-NH) contains an electronegative nitrogen atom, but it also donates electron density through resonance to the aromatic ring. The resonance effects partially counteracts the deshielding effect of the electronegative nitrogen making the chemical shifts in aryl amine-containing signals less deshielded compared to the nitro group. Meanwhile, C2/C2’, C3/C3’, C7/C7’, and C8/C8’ belonged to the methine carbons of the aromatic ring. These aromatic carbons resonated in the region of δ 130.24, 124.86, 120.61, and 114.97 ppm, respectively. C2/C2’ were more deshielded because they were closer to the nitro group compared to C3/C3’, C7/C7’, and C8/C8’.

The signal (C11) at *δ* 31.54 ppm indicated the presence of an ether bond in the compound. The carbon directly attached to the oxygen was slightly deshielded, but not as significantly as the carbonyl group carbon, owing to the electron donation effect of an oxygen atom. As a result, it had higher electron density, and the signal appeared in a moderately shielded region. Throughout the spectrum, signals appearing upfield commonly consisted of more shielded carbons. This was evident in the region of *δ* 28.88 – 29.22 ppm, which comprised carbon atoms attached to the alkyl chain (C13-C21), with the methylene having the strongest intensity. The most shielded carbon signal at δ 13.99 (C23), corresponded to the methyl group within the alkyl. Due to the NOE effect, the long alkyl chain exhibited the strongest intensities in the region, with spin-spin dipoles interacting through space [33]. The ^{13}C NMR chemical shift data for compound **2a** are tabulated in Table 3.

Table 3. The summarized ^{13}C NMR data for compound **2a**.

Carbon	Chemical Shift (ppm)
C1	145.90
C2/C2’	130.24
C3/C3’	124.86
C4	137.15
C5	162.52
C6	135.02
C7/C7’	120.61
C8/C8’	114.97
C9	143.32
C10	166.31
C11	31.54
C12	25.74
C13-C21	28.88-29.22
C22	22.27
C23	13.99

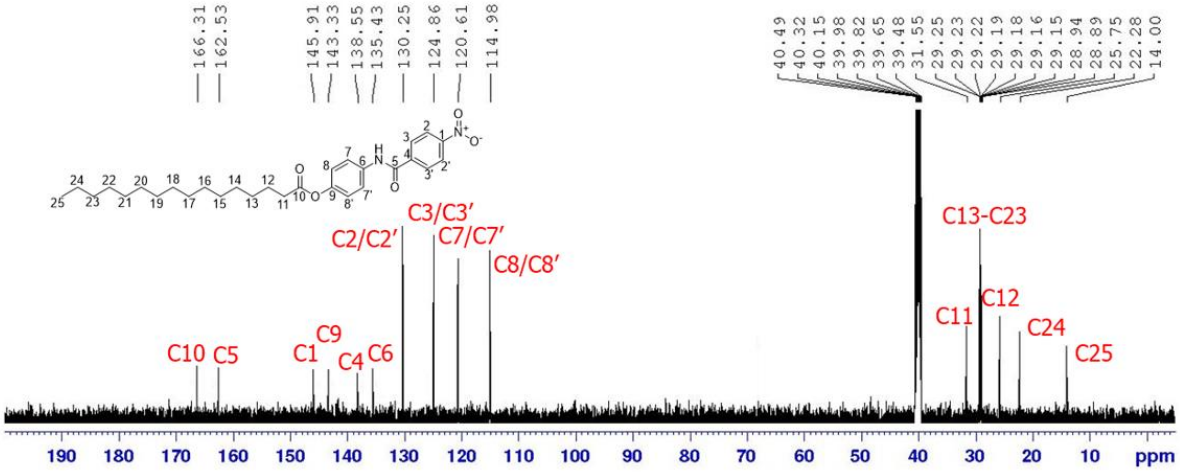

Figure 6. ^{13}C NMR (125 MHz, DMSO-d_6) spectrum of compound **2b**.

Table 4. CHN elemental analysis data for all compounds.

Compound	**% Found (Calculated)**		
	C (%)	**H (%)**	**N (%)**
1	60.35 (60.47)	3.85 (3.90)	10.79 (10.85)
2a	69.18 (69.21)	7.70 (7.74)	5.95 (5.98)
2b	70.08 (70.13)	8.11 (8.12)	5.60 (5.64)

Table 5. Phase sequence of intermediate **1** and compounds **2a-b**.

Compound	**Mode**	**Transition Temperature**
1	Heating	Cr→I 218.7°C
	Cooling	I→Cr 217.8°C
2a	Heating	Cr→I 180.5°C
	Cooling	I→Cr 178.7°C
2b	Heating	Cr→I 204.9°C
	Cooling	I→Cr 202.8°C

Notes: Cr=Crystal and **I**=Isotropic

To conclude, each signal in the ^{13}C NMR spectrum matched the projected structure of compound **2a**. The ^{13}C NMR spectrum of compound **2b** (Figure 6) also showed a similarity to that of compound **2a**, but had different intensities at the alkyl chain region. In other words, the longer the alkyl chain of a compound, the higher its signal intensity.

CHN Elemental Analysis

The percentage of carbon (C), hydrogen (H), and nitrogen (N) in intermediate **1** and compounds **2a** and **2b** are summarized in Table 4. The percentage errors for each compound were below 2 %, indicating that these compounds were of high purity.

Determination of Liquid Crystal Properties

Examination of the mesophase behaviour of the compounds was conducted using a polarized optical microscope (POM). The texture of phase transitions was observed under a microscope at a controlled temperature, and the collected data are given in Table 5. All the synthesized compounds were found to be non-mesogenic, without liquid crystal properties.

Table 5 indicates that all the compounds underwent direct isotropization and immediately transformed into a transparent isotropic liquid, without passing through liquid crystalline phases. Intermediate **1** exhibited the highest melting point among the three compounds, whereas compound **2a** had the lowest melting point. The higher transition and clearing temperatures observed in intermediate **1** may be attributed to the presence of a partial double bond in the amide connecting unit. Furthermore, the amide connecting unit's partial double bond nature contributed to increased rigidity, leading to elevated transition and clearing temperatures in the final compounds [34]. Consequently, there was a decrease in the Van der Waal forces between compounds. The increase in the terminal chain length leads to an elevation in cohesive forces, resulting in a higher melting point [35]. This was due to the requirement of additional energy to disrupt these bonds. As a result, no liquid crystal properties were exhibited by intermediate **1**.

Terminal substituents had a significant impact on molecular interactions. Intermediate **1**, which had small substituents like nitro and hydroxyl groups, was found to be non-mesogenic. Based on a previous study, the behaviour of small substituents such as chloro, nitro, hydroxy, and amino groups at the terminal end did not always form a liquid crystal phase [36]. The presence of a lone pair of electrons or *p* bonds in intermediate **1** led to resonance in the aromatic ring, causing the dipole moments of the molecules to cancel out. This decreased the polarizability and molecular interactions required for the development of mesophases [37], rendering this compound non-mesogenic.

The presence of a nitro group in a molecule reduces the flexibility of the chemical structure. This rigidity hinders the development of organized molecular structures required for liquid crystal behaviour. Molecules with rigid, rod-like structures typically exhibit higher transition temperatures, as their rigidity makes them less susceptible to thermal fluctuations that could otherwise disrupt the ordered structure. Therefore, increasing molecular rigidity generally raises the temperature at which these transitions occur [38]. Additionally, the presence of intramolecular hydrogen bonding between the hydroxy group and the carbonyl group imposes further limitations on the movement of molecules. The presence of hydrogen bonding results in a stronger internal connection within the molecule, which hinders these molecules from easily aligning and producing liquid crystal phases [39]. Consequently, compound **1** was unable to form a mesophase.

Compound **2b** exhibited a higher melting point than **2a** due to its longer alkyl chain. The alkyl chain with the greatest length has the highest transition temperatures [40]. The inclusion of more carbon chains resulted in higher transition temperatures for the compounds. Hence, the length of the alkyl group regulates the stability of the mesophase by impacting the magnitude of intermolecular interactions. Compounds possessing longer alkyl chains demonstrated enantiotropic mesophase, whereas compounds possessing shorter alkyl chains exhibited monotropic mesophase. Longer molecules tend to exhibit higher transition temperatures because the longer chains are more effective at forming ordered structures [41].

Even though intermediate **1** had an amide as a linking unit that resulted in a high melting temperature, it still did not exhibit mesophase. Meanwhile, both compounds **2a** and **2b** had low melting points compared to intermediate **1** due to their lower dipole moments. This was due to the ester linking unit, and could be related to the occurrence of resonance between the aromatic ring and the carbonyl oxygen that lowered the separation of charges along the compound [42].

Compounds **2a** and **2b** did not show any liquid crystal character, perhaps due to the lower conjugation, which maximized repulsive interactions between adjacent aromatic rings [43]. Increased conjugation generally improves the electronic delocalization and stability of a molecule [44]. Since compounds **2a** and **2b** had less conjugation, there were fewer interactions between molecules of aromatic rings that were close to each other, and thus, fewer repulsive forces. This diminished the tendency for mesophase formation, although compound **2b** had the highest melting temperature due to its longer alkane chain. The incorporation of elongated alkyl chains resulted in the disruption of linearity within this compound [45]. The lack of liquid crystal properties in these compounds can be ascribed to the nonlinearity present in their structures [46].

Finally, prior research has indicated that the inclusion of an amide group with an azo connecting unit resulted in compounds with mesogenic properties. Several research papers have also demonstrated the mesogenic properties of compounds that contain a Schiff base and amide as a connecting unit [47-49]. However, there has been less research published on the inclusion of an amide or ester as a connecting unit in liquid crystals. To exhibit liquid crystal qualities, certain compounds require a minimum of three aromatic rings, which could either be cycloaliphatic rings, or connected directly or through a suitable linking unit [50].

CONCLUSION

A series of new hybrid amide-ester derivatives were successfully synthesised. These derivatives were characterized using FTIR spectroscopy, NMR spectroscopy and CHN elemental analysis. The liquid crystal characteristics of the compounds produced were determined using polarized optical microscopy (POM). Observations revealed that none of these compounds displayed mesomorphic characteristics. The combined effects of resonance, structural rigidity from the nitro group, and intramolecular hydrogen bonding in intermediate **1** contributed to its inability to exhibit a mesophase. In addition, inclusion of an amide connecting unit resulted in intermediate **1** with small substituents like hydroxy and nitro groups having a significantly higher melting temperature. However, these compounds still did not exhibit liquid crystal behaviour, while possessing linear molecular structures and thermal stability. In addition, one reason why compounds **2a-b** did not induce mesophase may be due to their nonlinearity, caused by the loss of conjugation, thus making them less stable. There were fewer electronegative atoms attached, which led to the low polarizability of the compounds. Hence, enhancing these derivatives by modifying the terminal side arm with additional conjugation could further improve their properties. This approach involves introducing more conjugated systems, such as extended π-electron structures, into the side arm of the molecule. Furthermore, these derivatives bring together the unique properties of both amide and ester groups, allowing for customized molecular interactions. This could improve the performance and versatility of liquid crystal applications, such as displays, sensors, and optical devices. The ability to precisely control liquid crystal alignment and responsiveness could lead to significant advancements in performance and functionality.

ACKNOWLEDGEMENTS

The authors would like to acknowledge funding from Universiti Malaysia Sabah, Grant Number DKP0041 and SPB0004-2020; and lab facility support from Universiti Sains Malaysia.

The authors declare that they have no conflict of interest.

REFERENCES

1. Lagerwall, J. P. F. and Scalia, G. (2012) A New Era for Liquid Crystal Research: Applications of Liquid Crystals on Soft Matter Nano-, Bio- and Microtechnology. *Current Applied Physics*, **12**, 1387–1412.
2. Goossens, K., Lava, K., Bielawski, C. W. and Binnemans, K. (2016) Ionic Liquid Crystals: Versatile Materials. *Chemical Reviews*, **116**, 4643–4807.
3. Smith, C. (2018) A Review of Liquid Crystal Display Technologies, Electronic Interconnection and Failure Analysis. *Circuit World*, **34**, 35–41.
4. Ma, J. and Xuan, L. (2013) Towards Nanoscale Molecular Switch-Based Liquid Crystal Displays. *Displays*, **34**, 293–300.
5. Carlton, R. J., Hunter, J. T., Miller, D. S., Abbasi, R., Mushenheim, P. C., Na Tan, L. and Abbott, N. L. (2013) Chemical and Biological Sensing using Liquid Crystals. *Liquid Crystals Reviews*, **1**, 29–51.
6. Jamain, Z., Azman, A. N. A., Razali, N. A. and Makmud, M. Z. H. (2022). A Review on Mesophase and Physical Properties of Cyclotriphosphazene Derivatives with Schiff Base Linkage. *Crystals*, **12**, 1174.
7. Andrienko, D. (2018) Introduction to liquid crystals. *Journal of Molecular Liquids*, **267**, 520–541.
8. Kashyap, D., Patel, S., Prajapat, V., Sharma, V. and Vasava, D. (2019) Effect of the linking unit on the calamitic-shaped liquid crystal: a comparative study of two homologous series of benzoate and cinnamate linked compounds. *Molecular Crystals and Liquid Crystals*, **681**, 58–70.
9. Kaur, S., Punjani, V., Yadav, N., Barthakur, A., Baghla, A., Dhara, S. and Pal, S. K. (2022) Chemical and Physical Aspects of Recent Bent-Shaped Liquid Crystals Exhibiting Chiral and Achiral Mesophases. *Liquid Crystals*, **49**, 1078–1146.
10. Václav, K., Martin, H., Jiří, S., Vladimíra, N. and Damian, P. (2012) 3-Aminophenol based bent-shaped liquid crystals with an amide linking group. *Liquid Crystals*, **39**, 943–955.
11. Karanlık, G., Ocak, H. and Bilgin Eran, B. (2019) Imine Based Chiral Liquid Crystals: Effect of Varying The Terminal Substituent and Orientation of Ester Linking Unit. *Journal of Molecular Liquids*, **275**, 567–577.
12. Jamain, Z., Khairuddean, M., Zulbaharen, N. N., Chung, T. K. (2019) Synthesis, characterization and determination of mesophase transition of azo-azomethine derivatives with different terminal chain lengths. *Malaysian Journal of Chemistry*, **21**, 73–85.
13. Levine, A. W. (1975) Structure-Property Relationships in Thermotropic Organic Liquid Crystals. In: Priestley, E.B., Wojtowicz, P.J., Sheng, P. (eds) Introduction to Liquid Crystals. *Springer, Boston, MA*.
14. Nessim, R. I., Naoum, M. M., Mohamed, S. Z. and Nessim, M. I. (2004) Effect of molecular structure on the phase behaviour of some liquid crystalline compounds and their mixtures XIII. 4-(4-Substituted phenylazo)phenyl 4-alkoxybenzoates. *Liquid Crystals*, **31**, 649–654.
15. Jamain, Z., Habil, S., Makmud, M. Z. H. and Khairuddean, M. (2021) Synthesis, Structural and Dielectric Characteristics of Liquid Crystalline Azo-Based Compounds with Different Terminal Length. In Proceedings of the 2021 IEEE. *International Conference on the Properties and Applications of Dielectric Materials (ICPADM), Johor Bahru, Malaysia*, 12–14 July 2021, 49–52.
16. Shanker, G., Kumar, K. R. S. and Paul, B. (2022) Perspective on Structure-Property Relationship of Room Temperature Single-Component Liquid Crystals. *Liquid Crystals*, **49**, 1545–1603.
17. Habil, S., Jamain, Z. and Makmud, M. Z. H. (2024) Synthesis and Characterization of Azo-Based Cyclotriphosphazene Compounds: Liquid Crystalline and Dielectric Properties. *Chem-Engineering*, **8**, 71.
18. Davarci, D. and Doganci, S. (2022) Liquid Crystal Phosphazenes. *Journal of Molecular Structure*, **1269**, 1–18.
19. Jamain, Z., Khairuddean, M. and Guan-Seng, T. (2020) Synthesis of Novel Liquid Crystalline and Fire Retardant Molecules Based on Six-Armed Cyclotriphosphazene Core Containing Schiff Base and Amide Linking Units. *RSC Advances*, **10**, 28918–28934.
20. Wu, W. N., Jiang, Y. M., Fei, Q., Du, H. T. and Mao-Fa Yang, M. F. (2020) Synthesis and Antifungal Activity of Novel 1,2,4-Triazole Derivatives Containing an Amide Moiety. *Journal of Heterocyclic Chemistry*, **57**, 1379–1386.
21. Zulaziz, N. A. S., Jamain, Z. and Khairuddean, M. (2024) Synthesis, Characterization, and

Liquid Crystalline Behavior of Ester-Schiff Base Derivatives Attached to Nonyl and Tetradecyl Terminal Chains. *Malaysian Journal of Chemistry*, **26**, 572–582.

22. Jevtovic, V., Ahmed, H. A., Khan, M. T., Al Zahrani, S. A., Masood, N., Jeilani, Y. A. (2023) Preparation of Laterally Chloro-Substituted Schiff Base Ester Liquid Crystals: Mesomorphic and Optical Properties. *Crystals*, **13**, 835.
23. Lewis, W. (1972) Ultraviolet Spectroscopy. Paint Testing Manual. Ed. Sward, G. 100 Barr Harbor Drive, PO Box C700, West Conshohocken, PA 19428–2959: *ASTM International*.
24. Gupta, P., Das, S. S. and Singh, N. B. (2023) Spectroscopy (1st ed.). *Jenny Stanford Publishing*.
25. Mohamad Fazli, F. J., Jamain, Z. (2024) Synthesis and Characterization of Hydrazine Bridge Cyclotriphosphazene Derivatives with Amide–Schiff Base Linkages Attached to Decyl and Hydroxy Terminal Groups. *Molbank*, **2024**, M1934.
26. Saito, K., Xu, T. & Ishikita, H. (2022) Correlation between C═O Stretching Vibrational Frequency and p*k*a Shift of Carboxylic Acids. *The Journal of Physical Chemistry B*, **126**, 4999–5006.
27. Jamain, Z., Khairuddean, M. & Guan-Seng, T. (2020) Synthesis of New Star-Shaped Liquid Crystalline Cyclotriphosphazene Derivatives with Fire Retardancy Bearing Amide-Azo and Azo-Azo Linking Units. *International Journal of Molecular Sciences*, **21**, 4267.
28. Yamaguchi, I. (1963) Magnetic Anisotropy of the Nitro Group Studied by Nuclear Magnetic Resonance. *Molecular Physics*, **6**, 105–114.
29. Kupka, T., Dziuk, B., Ejsmont, K., Makieieva, N., Fizer, L., Monka, N., Konechna, R., Stadnytska, N., Vasyliuk, S. and Lubenets, V. (2024) Impact of Crystal and Molecular Structure of Three Novel Thiosulfonate Crystals on Their Vibrational and NMR Parameters. *Journal of Molecular Structure*, **1313**, 138642.
30. Jaeger, M. and Aspers, R. L. E. G. (2012) Steroids and NMR. *Annual Reports on NMR Spectroscopy*, 115–258.
31. Usri, S. N. K., Jamain, Z. and Makmud, M. Z. H. (2022) Fire Retardancy and Dielectric Strength of Cyclotriphosphazene Compounds with Schiff Base and Ester Linking Units Attached to the Electron-Withdrawing Side Arm. *Polymers*, **14**, 4378.
32. Katritzky, A. R., Ramsden, C. A., Joule, J. A. and Zhdankin, V. V. (2010) 4.1-Overview. *Handbook of Heterocyclic Chemistry (Third Edition)*, 641–651.
33. Kara, Y. S. and Diran, D. (2024) Synthesis of Novel 1,2,4-Oxadiazine Derivatives and The Substituent Effect Study on ^{13}C NMR Spectra. *Journal of Molecular Structure*, **1310**, 138309.
34. Jamain, Z., Khairuddean, M., Kamaruddin, K. and Rui, Y. Z. (2021) Synthesis, Structural Elucidation and Mesophase Behaviour of Hexasubstituted Cyclotriphosphazene Molecules with Amide Linking Unit. *Malaysian Journal of Chemistry*, **23**, 213–225.
35. Jamain, Z. and Khairuddean, M. (2021) Synthesis and Mesophase Behaviour of Benzylidene-Based Molecules containing Two Azomethine Units. *Journal of Physics: Conference Series*, **1882**, 012120.
36. Nawawi, M. F., Salleh, N. M., Lee, V. S., Cheng, S. -F. (2023) Synthesis, Characterization and Structure-Mesomorphic Properties Relationship of Palm-Based Azo-Ester Bridged Liquid Crystals from Caprylic Acid. *Industrial Crops and Products*, **199**, 116765.
37. Jamain, Z., Omar, N. F. and Khairuddean, M. (2020) Synthesis and Determination of Thermotropic Liquid Crystalline Behavior of Cinnamaldehyde-Based Molecules with Two Schiff Base Linking Units. *Molecules*, **25**, 3780
38. Sharma, V. S. and Patel, R. B. (2016) Molecular Structure and Mesomorphism: Effect of Tail/ Lateral Group. *Molecular Crystals and Liquid Crystals*, **630**, 58–68.
39. Martínez-Felipe, A. and Imrie, C. T. (2015) The Role of Hydrogen Bonding in The Phase Behaviour of Supramolecular Liquid Crystal Dimers. *Journal of Molecular Structure*, **1100**, 429–437.
40. Markiewicz, R., Klimaszyk, A., Jarek, M., Taube, M., Florczak, P., Kempka, M., Fojud, Z. and Jurga, S. (2021) Influence of Alkyl Chain Length on Thermal Properties, Structure, and Self-Diffusion Coefficients of Alkyltriethylammonium-Based Ionic Liquids. *International Journal of Molecular Sciences*, **22**, 5935.
41. Jamain, Z., Khairuddean, M., Loh, M. L., Manaff, N. L. A. and Makmud, M. Z. H. (2020) Synthesis and Characterization of Hexasubstituted Cyclotriphosphazene Derivatives with Azo Linking Units. *Malaysian Journal of Chemistry*, **22**, 125–140.
42. Nada, S., Hagar, M., Farahat, O., Hasanein, A. A., Emwas, A. H., Sharfalddin, A. A., Jaremko, M. and Zakaria, M. A. (2022) Three Rings Schiff

Base Ester Liquid Crystals: Experimental and Computational Approaches of Mesogenic Core Orientation Effect, Heterocycle Impact. *Molecules*, **27**, 2304.

43. Mali, A. A. A. and Jamain, Z. (2023) Synthesis and Characterization of Non-mesogenic Behavior of Chalcone Derivatives. *Malaysian Journal of Chemistry*, **25**, 158–168.

44. Valadbeigi, Y. (2018) Comparison of Effects of Charge Delocalization and Π-Electron Delocalization on The Stability of Monocyclic Compounds. *Journal of Molecular Graphics and Modelling*, **80**, 104–112.

45. Katariya, K. D., Nakum, K. J., Soni, H., Nada, S., Mohamed Hagar, M. (2023) Imine Based Fourring Chalcone-Ester Liquid Crystals: Synthesis, Characterization, Mesomorphic Behavior and DFT Approach. *Journal of Molecular Liquids*, **380**, 121719.

46. Fadhil, M. Z. A. M., Mustamin, M. A. and Jamain, Z. (2024) Liquid Crystalline Behaviour of Symmetrical Thermotropic Schiff Base Compounds. *Journal of Molecular Structure*, **1315**, 138929.

47. Joshi, V. K., Katariya, K. D. and Nakum, K. J. (2024) Synthesis, Mesomorphic Behaviour, and DFT Studies of Biphenyl Bis-Ester Schiff Base Liquid Crystals. *Journal of Molecular Structure*, **1311**, 138338.

48. Amiruddin, N. S., Jamain, Z. and Khairuddean, M. (2023) Synthesis, Characterization and Liquid Crystalline Behavior of 4-((E)-(((E)-4-(Decyloxy) Benzylidene) Hydrazineylidene)Methyl)Phenol. *Malaysian Journal of Chemistry*, **25**, 517–524.

49. Ahmed, H., Hagar, M. and Saad, G. (2019) Impact of The Proportionation of Dialkoxy Chain Length on The Mesophase Behavior of Schiff Base/Ester Liquid Crystals; Experimental and Theoretical Study. *Liquid Crystals*, **46**, 1611–1620.

50. Guardià, J., Reina, J. A., Giamberini, M. and Montané, X. (2024) An Up-to-Date Overview of Liquid Crystals and Liquid Crystal Polymers for Different Applications: A Review. *Polymers*, **16**, 2293.